Available online at www.sciencedirect.com
SCIENCE DIRECT®
ELSEVIER
Journal of Magnetism and Magnetic Materials 293 (2005) 526–531
Journal of magnetism and magnetic materials
www.elsevier.com/locate/jmmm

Magnetic resonance of magnetic fluid and magnetoliposome preparations

Paulo C. Morais[a,*], Judes G. Santos[a], K. Skeff Neto[a], Fernando Pelegrini[b], Marcel De Cuyper[c]

[a] *Universidade de Brasília, Instituto de Física, Núcleo de Física Aplicada, 70919-970 Brasília-DF, Brazil*
[b] *Universidade Federal de Goiás, Instituto de Física, 74001-970 Goiânia-GO, Brazil*
[c] *Katholieke Universiteit Leuven, Campus Kortrijk, Interdisciplinary Research Centre, B-8500 Kortrijk, Belgium*

Available online 3 March 2005

Abstract

In this study, magnetic resonance was used to investigate lauric acid-coated magnetite-based magnetic fluid particles and particles which are surrounded by a double layer of phospholipid molecules (magnetoliposomes). The data reveal the presence of monomers and dimers in both samples. Whereas evidence for a thermally induced disruption of dimers is found in the magnetic fluid, apparently, the bilayer phospholipid envelop prevents the dissociation in the magnetoliposome samples.

Keywords: Magnetic resonance (MR); Magnetic fluid; Magnetoliposome; Dimer disruption

Magnetic fluids (MFs) are stable colloidal suspensions containing surface-dressed nanosized magnetic particles suspended either in an organic or inorganic carrier fluid [1]. As far as the magnetizable colloidal structures are concerned, magnetoliposomes (MLs) take a special place. The coating, indeed, consists of phospholipids which adopt a bilayer configuration [2], as encountered in natural membranes. As a result, the particles are completely biocompatible and are successfully used in a variety of in vivo setups, e.g. as drug-delivery systems [3], as magnetic resonance imaging markers for cancer diagnosis [4] and in cancer therapy [5]. A whole battery of methods such as high-resolution microscopy and magnetization measurements [6], static magnetic birefringence [7], and Raman spectroscopy [8] are currently used to characterize various physico-chemical properties of MLs. Also, magnetic resonance (MR) has been shown to be a powerful method to investigate magnetic nanoparticles dispersed in a non-magnetic matrix [9]; in particular, to investigate several

*Corresponding author. Tel.: +55 61 2736655; fax: +55 61 2723151.
E-mail address: pcmor@unb.br (P.C. Morais).

0304-8853/$ - see front matter © 2005 Elsevier B.V. All rights reserved.
doi:10.1016/j.jmmm.2005.01.069

aspects of ionic [10], surface-coated [11], and biocompatible [12] MFs. In addition, MR has been recently used as an important spectroscopic technique to investigate the biodistribution of magnetic nanoparticles intravenously injected in animals [13]. In the present study, MR measurements have been used to investigate the temperature dependence of both the resonance field and the resonance linewidth of a MF sample and the counterpart ML sample.

Preparation of both the laurate-coated magnetite-based aqueous MF sample and the ML sample, derived from the MF sample, was performed according to the standard procedure described earlier in the literature by De Cuyper and Joniau [2]. As obtained from transmission electron microscopy (TEM) micrographs, the average diameter and the diameter dispersion (lognormal distribution function) of the iron oxide nanoparticle were 9.4 nm and 0.30, respectively. The nanoparticle concentration in the stock samples (ML and MF) was about 3×10^{21} particles/m^3. Nanoparticle concentration was estimated by combining the average particle diameter (TEM data) with chemical analysis performed using atomic absorption data. Dilution of the stock samples was performed with distilled water. The magnetic nanoparticle concentration in both the ML and the MF samples used to record the MR spectra spans from 2.4×10^{19} to 2.4×10^{21} particles/m^3. The resonance system used to perform the experiments was a commercial Brucker ESP-300 spectrometer operating in the X-band region (about 9.4 GHz). MR measurements as a function of temperature (in the range of 100–270 K) were done on samples (MF and ML) containing 2.4×10^{21} particles/m^3. In this case, the samples were frozen under zero-field condition. The MR spectra were then recorded by heating the samples from lower (100 K) to higher temperatures (270 K).

Fig. 1 shows typical room-temperature MR spectra of the MF and ML samples, at three different particle concentrations (2.4×10^{19}, 2.4×10^{20}, and 2.4×10^{21} particles/m^3). Note that the MR spectra in Fig. 1 are the first derivative of the microwave absorption signal and show visible asymmetric shapes. Such asymmetry indicates the

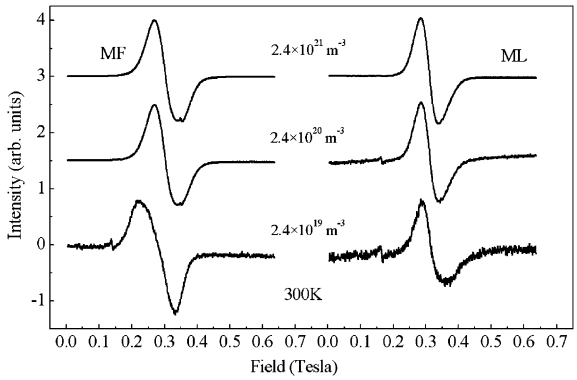

Fig. 1. Typical room-temperature MR spectra of MFs and MLs at particle concentrations of 2.4×10^{19}, 2.4×10^{20}, and 2.4×10^{21} particles/m^3.

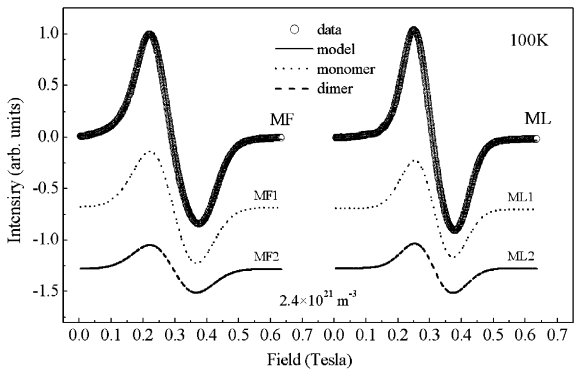

Fig. 2. Fitting of the low-temperature (100 K) MR spectra (MF and ML) using two components to account for monomers and dimers.

presence of different magnetic structures (monomers and agglomerates), as previously reported for MF samples [11]. Therefore, all the MR spectra were curve fitted using two Gaussian-shaped components, accounting for monomer and dimer, as discussed in more detail later on in this study. Fig. 2 shows typical curve fittings of the MR spectra of the concentrated (2.4×10^{21} particles/m^3) MF and ML samples at 100 K: the two Gaussian-shaped components (dashed and dotted lines), the best fit of the experimental data (solid line), and the experimental data (symbols) are depicted.

Fig. 3 shows the temperature (T) dependence of the resonance field (H_R) of both MF and ML

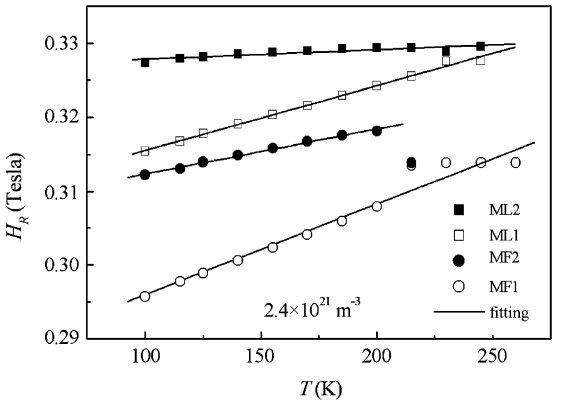

Fig. 3. Temperature dependence of the resonance field of the two components (monomer and dimer), for the two samples MF and ML.

samples containing 2.4×10^{21} particles/m^3. The two Gaussian-like components associated to the MF resonance spectra are labeled MF1 (○) and MF2 (●), corresponding to the low-field and high-field lines, respectively. At 100 K, the MF1 and MF2 components contribute to the fitted spectrum with 68% and 32%, respectively (see Fig. 2). Likewise, the low-field and high-field Gaussian-like components associated to the ML resonance spectra are labeled ML1 (□) and ML2 (■), respectively. Similarly, at 100 K, the ML1 and ML2 components contribute to the fitted spectrum with 62% and 38%, respectively (see Fig. 2). Note that static magnetic birefringence has been previously used to investigate the amount of monomers and dimers in samples of MFs and MLs containing smaller magnetite nanoparticles [7]. In contrast to the MR data presented in this study, the magnetic birefringence data reported in Ref. [7] showed that the amount of dimers is higher than that of monomers. Such a difference, however, could be due to differences in the experimental technique (MR versus birefringence) and/or differences in average particle diameter (about twice). Except for the MF2 component (●), all the H_R versus T data points can be fitted by a straight line in the whole range of temperature investigated. At about 210 K the MF2 component (●) shifts downwards and merges with the MF1 component (○). As previously reported for ionic magnetic fluids [14], this observed abrupt shift of the MF2 component (●) around 210 K can be assigned to a thermally induced dimer disruption. In contrast, within the same temperature range, such a drastic deviation from linearity is not observed for the MR components ML1 (□) and ML2 (■). Consequently, based on these observations as well as on data from the literature [11,14] we suggest that the MF1 and MF2 components represent monomers and dimers, respectively. From the ML H_R versus T graph, it further appears that such a presumed dimer disruption does not occur with MLs. This can be easily understood by assuming that once the magnetic nanoparticles are coupled together as a dimer inside the magnetoliposome structure, then are tightly held together by the phospholipid bilayer. The quantitative analysis of the H_R versus T data, presented in this study, further supports this picture.

In support of the observations reported in the present study as well as in our previous investigations [11,14], we should emphasize that magnetic nanoparticle chain formation has been long ago predicted by theoretical analysis [15]. More recently, however, cryogenic electron microscopy has been used to directly observe chains of magnetic nanoparticles in magnetic fluid samples [16,17].

To explain the temperature dependence of the resonance field (see Fig. 3), the resonance frequency ω_R, i.e. the Larmor precession frequency of the nanoparticle magnetic moment in the presence of an effective magnetic field (H_{EFF}), is written as $\omega_R = \gamma H_{EFFF}$, where γ is the gyromagnetic ratio. The effective magnetic field may be well described as a result of three main components, namely, the external sweeping field (H_E), the demagnetizing field (H_D), and the anisotropy field (H_A). At the resonance condition, H_E matches the resonance field (H_R), which is described [10] by

$$H_R = \omega_R/\gamma - H_D - H_A. \quad (1)$$

Inspection of Eq. (1) suggests that the temperature dependence of the resonance field is mainly associated to the last term on the right-hand side (H_A), through its dependence upon the effective magnetocrystalline anisotropy density (K_{EFF}), as follows. The anisotropy field in spherical magnetite nanoparticles is given by $H_A = 2K_{EFF}/M_S$,

where M_S is the saturation magnetization. In magnetic nanoparticles the effective anisotropy energy density has both bulk (K_B) and surface (K_S) components, i.e. $K_{EFF} = K_B + K_S$. The surface component is related to the surface-to-volume ratio by $K_S = (6/D)k_S$, where D is the nanoparticle diameter and k_S is the surface anisotropy [18]. In general, K_{EFF} and M_S are both temperature dependent. However, considering that our data were taken far below the Curie point for bulk magnetite (850 K), M_S could be taken as approximately flat (470 kA/m). Therefore, the temperature dependence of the anisotropy field would follow mainly the temperature dependence of the effective magnetic anisotropy. Inspection of the points in Fig. 3 shows a linear relationship between H_R and T. In other words, the effective magnetic anisotropy would be empirically represented by $K_{EFF} = K_0 + k_{EFF}T$. K_0 is a constant and k_{EFF} is a size-dependent coefficient, expressed in units of $J/m^3\,K$. Straight lines in Fig. 3 represent the best fit of the data using the empirical relation $H_R = B + AT$, where $A = 2k_{EFF}/M_S$ is the slope and $B = (\omega_R/\gamma - 2K_0/M_S - H_D)$ the intercept constant. Comparing the empirical relation $K_{EFF} = K_0 + k_{EFF}T$ with $K_{EFF} = K_B + K_S$, one identifies K_0 with K_B and $k_{EFF}T$ with $(6/D)k_S$. At this point we argue that k_{EFF} is directly proportional to $6/D$.

Fitting of the magnetic resonance data (solid lines in Fig. 3) shows that the value of A for the MF1 component (119.4 kA/m K) is about twice the value of A for the MF2 component (63.7 kA/m K), whereas B is lower for the MF1 component (224.4 kA/m) in comparison to the MF2 component (240.0 kA/m). Note that the ratio of the slope values found for MF1 and MF2 (about 2) supports the proposed picture of monomer and dimer associated to the MF1 and MF2 components, respectively. This is because the slope (A) is inversely related to the magnetic nanoparticle diameter ($6/D$). Alternatively, values obtained for the intercept constant ($\omega_R/\gamma - 2K_0/M_S - H_D$) depend mainly upon the values of the demagnetizing field for monomer and dimer which are $H_D = (4\pi/3)M_S$ and $H_D = (N_\perp - N_\parallel)M_S$, respectively. For spheroids, the $N_\perp$; and $N_\parallel$ demagnetizing tensor components equal $N_\perp = [4\pi q^2/(q^2-1)]\{1 - (q^2-1)^{-1/2}\arcsin[q^{-1}(q^2-1)^{1/2}]\}$ and $N_{||} = [(4\pi - N_\perp)/2]$, where $q = 2$ for the dimer [19]. Therefore, the calculated difference in B values associated to monomer and dimer is about 23.2 kA/m. Note that the fitted values for B associated to MF1 and MF2 components give a difference of only 15.6 kA/m. This observed discrepancy of 7.6 kA/m, however, could be due to differences in the saturation magnetization between monomer and dimer.

Analysis of the A and B values found from the ML resonance data points to similar conclusions. The ratio of the slopes associated to the ML1 component (103.5 kA/m K) and ML2 component (47.7 kA/m K) is about 2.2, basically suggesting the occurrence of monomers (ML1) and dimers (ML2), too. Likewise, the difference between the fitted values for B associated to the ML1 component (249.3 kA/m) and the ML2 component (259.3 kA/m) is about 10 kA/m. Again, the observed difference (13.2 kA/m) can be ascribed to differences in the saturation magnetization between monomer and dimer in the ML structure. Finally, it should be stressed that the A values fitted for the MF1 and ML1 components do not differ significantly (119.4 versus 103.5 kA/m K), indicating a similar magnetic structure (monomer). In an analogous way, the A values fitted for the MF2 and ML2 components, too, are nearly very much close together (63.7 versus 47.7 kA/m K), suggesting a similar magnetic structure (dimer).

Fig. 4 represents the experimental values of the temperature (T) dependence of the MR linewidth (ΔH_R). The ΔH_R versus $1000/T$ data resemble the picture of an ensemble of magnetic nanoparticles dispersed in a non-magnetic matrix, in which the resonance linewidth broadening is expressed [20] by

$$\Delta H_R = \Delta H_{R0}\tanh(K_{EFF}V/2kT), \quad (2)$$

where $V = (\pi/6)D^3$ is the particle volume, $\Delta H_{R0} = 5g\beta Sn/d^3$, and $\Delta E = K_{EFF}V$ is the energy barrier (height) mainly associated to the magnetic anisotropy. The description of the pre-factor (ΔH_{R0}) in Eq. (2) includes the g-factor (g), the Bohr magneton (β), the spin associated with each magnetic center inside the nanoparticle (S), the number of magnetic centers per magnetic nanoparticle (n), and the average distance between adjacent magnetic structures in the non-magnetic matrix (d). Except for the MF2 component, the

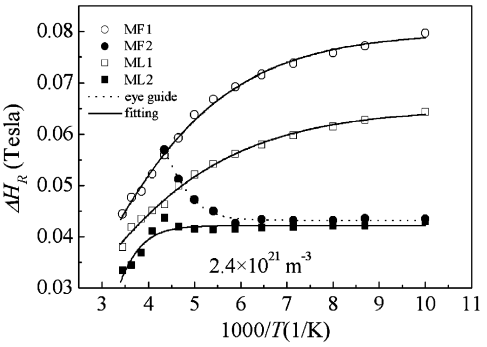

Fig. 4. Temperature dependence of the resonance linewidth of the two components (monomer and dimer), for the two MF and ML samples. Note the inverse of the absolute temperature scale on the horizontal axis.

data shown in Fig. 4 reveal the classical/standard behavior, i.e. a linewidth narrowing as the temperature increases [20]. The usual ΔH_R versus $1000/T$ behavior is due to the functional dependence ($K_{EFF}V/2kT$) of the hyperbolic function in Eq. (2). Note that the solid lines in Fig. 4 show excellent agreement between the resonance linewidth data (MF1, ML1, and ML2 components) and the temperature dependence provided by Eq. (2). The ΔH_R versus $1000/T$ data related to the MF2 component, however, are quite different from the ΔH_R versus $1000/T$ data related to the other three MR components. Fig. 4 shows that the linewidth associated to the MF2 component goes approximately flat up to about 170 K, above which the MF2 component broadens until it coincides with that observed for the MF1 component at about 250 K. As already claimed in this study and in accordance with the H_R versus T behavior (see the MF2 component in Fig. 3), the anomalous behavior of the ΔH_R versus $1000/T$ data associated to the MF2 component is due to dimer disruption in the temperature range of about 170–250 K. For the magnetoliposome population, however, no signal of dimer dissociation is expected in the H_R versus T graph as long as the ML is structurally preserved. Inspection of Eq. (2), however, shows that the hyperbolic function's argument ($K_{EFF}V/2kT$) affects the resonance linewidth value (ΔH_R) through the effect of the temperature, whereas the pre-factor ($\Delta H_{R0} = 5g\beta Sn/d^3$) influences the ΔH_R saturation value through the effective magnetic moment associated to the magnetic structure ($g\beta Sn$) [20]. Concerning the effect of the effective magnetic moment (vector sum) associated to the dimer structure in the fanning configuration, we note that it could be smaller than the magnetic moment associated to the monomer. The ratio (monomer over dimer) of the observed saturation linewidth values (ΔH_{R0}) associated to the MF (1.84) and ML (1.53) samples allow us to estimate the angle between the two magnetic moments in the dimer (fanning configuration) equal to 148° and 142°, respectively. These values are higher than the 98° value calculated for the dimer of uncoated nanoparticles. We claim that the non-spherical shape of the nanoparticles surface molecular coating may account for the shift from 98° to 148° (dimer in the MF sample) and 142° (dimer in the ML sample), with remarkable influence on the effective magnetic moment associated to the dimer structure. Indeed, the values we found for S, g, D, and K_{EFF} by fitting of the ΔH_R versus $1000/T$ data according to Eq. (2) are all quite reasonable. The S (from 1.99 to 2.15) and g (from 1.87 to 2.10) values are in very good agreement with octahedral Fe^{2+} ions ($3d^6$ configuration) in the crystal unit cell of magnetite. Furthermore, the D values (from 9.6 to 10 nm) are almost identical to the average diameter value obtained from TEM data (9.4 nm). The K_{EFF} values (1.2×10^4–1.4×10^4 J/m^3) obtained from the fitting of the data shown in Fig. 4, however, are twice the value quoted in the literature for bulk magnetite (0.6×10^4 J/m^3). Nevertheless, such discrepancy can be expected for nanosized magnetic particles due to the strong surface anisotropy contribution [21].

In summary, a magnetic fluid sample and a magnetoliposome sample were systematically investigated using temperature variable magnetic resonance (X-band) measurements. The magnetic resonance lineshape analyses indicate two components for both magnetic fluid and magnetoliposome samples. Analysis of the resonance field versus temperature data performed for each line component strongly supports the picture of the occurrence of monomers and dimers in both samples. A strong

indication for a thermally induced dimer disruption in the magnetic fluid sample can be deduced from the collapses of the two resonance components around 210 K. The resonance linewidth versus temperature data are well explained within the model of magnetic nanoparticles dispersed in non-magnetic templates. As far as the temperature dependence of the resonance linewidth is concerned, we observed quite different trends for monomers and dimers. For both magnetic fluid and magnetoliposome samples the magnetic resonance linewidth associated to monomers shows the standard behavior, i.e. the linewidth decreases as the temperature increases. In the case of dimers, the situation is quite different, i.e. in the magnetoliposome sample the standard behavior is observed, whereas, in contrast, in the magnetic fluid sample the resonance linewidth increases as the temperature increases. Again, such anomalous behavior associated to the dimer component of the magnetic fluid sample is seen as the signature of the dimer disruption. Finally, the absence of the signature of dimer disruption in the magnetoliposome resonance data (resonance field and resonance linewidth) is a strong indication that the phospholipid bilayer prevents dimer disruption in the temperature range of our experiment. This fact may have a strong influence upon the magnetohyperthermia effect for instance, once the magnetic peak susceptibility of dimers could be quite different from the magnetic peak susceptibility of monomers, as reported in Ref. [7].

Financial support for this study was provided by the Brazilian agencies CNPq, FINATEC, and the Flemish Fonds voor Wetenschappelijk Onderzoek.

References

[1] R. Massart, IEEE Trans. Magn. 17 (1981) 1247.
[2] M. De Cuyper, M. Joniau, Eur. Biophys. J. 15 (1988) 311.
[3] H. Chen, R. Langer, Pharmac. Res. 14 (1997) 537.
[4] S. Päuser, R. Reszka, S. Wagner, et al., Anti-Cancer Drug Des. 12 (1997) 125.
[5] A.A. Kuznetsov, V.I. Filippov, et al., J. Magn. Magn. Mater. 225 (2001) 95.
[6] M. De Cuyper, P. Müller, H. Lueken, et al., J. Phys. C: Condens. Matter 15 (2003) S1425.
[7] P.C. Morais, K. Skeff Neto, P.P. Gravina, J. Magn. Magn. Mater. 252 (2002) 418.
[8] M.A.G. Soler, S.W. da Silva, T.F.O. Melo, et al., J. Magn. Magn. Mater. 252 (2002) 415.
[9] R.S. De Biasi, T.C. Devezas, J. Appl. Phys. 49 (1978) 2466.
[10] O. Silva, E.C.D. Lima, P.C. Morais, J. Appl. Phys. 93 (2003) 8456.
[11] P.C. Morais, G.R.R. Gonçalves, K. Skeff Neto, et al., IEEE Trans. Magn. 38 (2002) 3225.
[12] L.M. Lacava, Z.G.M. Lacava, M.F. Da Silva, et al., Biophys. J. 80 (2001) 2483.
[13] L.M. Lacava, Z.G.M. Lacava, et al., J. Magn. Magn. Mater. 252 (2002) 367.
[14] P.C. Morais, G.R.R. Gonçalves, et al., J. Magn. Magn. Mater. 225 (2001) 84.
[15] P.G. De Gennes, P.A. Pincus, Phys. Kondens. Mater. 11 (1970) 189.
[16] K. Butter, P.H.H. Bomans, P.M. Frederik, et al., Nature Mater. 2 (2003) 88.
[17] K. Butter, P.H.H. Bomans, et al., J. Phys. C: Condens. Matter 15 (2003) S1451.
[18] F. Bodker, S. Morup, S. Linderoth, Phys. Rev. Lett. 72 (1994) 282.
[19] R.C. O'Handley, Modern Magnetic Materials: Principles and Applications, Wiley, New York, 2000.
[20] P.C. Morais, M.C.F.L. Lara, A.L. Tronconi, et al., J. Appl. Phys. 79 (1996) 7931.
[21] A.F. Bakuzis, P.C. Morais, F. Pelegrini, J. Appl. Phys. 85 (1999) 7480.